# Electronic Supplementary Information

## Chemical Communications

# Enhanced proton conductivity in amino acid based self-assembled non-porous hydrogen-bonded organic frameworks

*Titas Pramanik,*[a] Ashish Anand,[a] Ajmal Pandikassala,[b,c] Rajith Illathvalappil, [b,c] Sreekumar Kurungot, [b,c] T. N. Guru Row*[a]*

[a]Solid State and Structural Chemistry Unit, Indian Institute of Science, Bengaluru 560012, Karnataka, India

[b]Physical and Materials Chemistry Division, CSIR-National Chemical Laboratory, Pune, Maharashtra, 411008, India

[c]Academy of Scientific and Innovative Research (AcSIR), Ghaziabad-201002, India

AUTHOR INFORMATION

**Corresponding Authors**

**T. N. Guru Row -** *email: gururow@iisc.ac.in*

**Titas Pramanik -** *email: titaspramanik1990@gmail.com*

## Experimental Section

**Materials Preparation:** β-alanine, glycine, and L-leucine were purchased from Sisco Research Laboratories Pvt. Ltd. (India). Oxalic acid monohydrate was purchased from SDFCL (India). All the chemicals were used without further purification. **BALAOA**, **GLYOA**, and **LEUOA** samples were produced in bulk by liquid assisted (water and methanol mixtures) mechanical grinding of β-alanine, glycine, and L-leucine with oxalic acid monohydrate in 1:1 stoichiometric ratio. All the bulk powder samples were characterized by Profile-fitting analysis of the recorded PXRD patterns. Reported single crystal structure parameters for each of these samples were used for the refinement. Single crystals of **BALAOA**[1], **GLYOA**[2], and **LEUOA**[3] were obtained by crystallization of the powder samples from saturated aqueous solution.

**Single Crystal X-ray Diffraction (SCXRD) Experiments:** Diffraction quality single crystals of **BALAOA** were selected using a polarizing microscope. Single crystal X-ray diffraction data was collected on an Oxford Xcalibur Mova E diffractometer equipped with EOS CCD detector, and a micro focus sealed tube using Mo Kα radiation (λ = 0.71073 Å). The data collections were done at 100 K using a liquid nitrogen gas stream cooling device. Cell refinement, data integration, and reduction were carried out using the program *CrysalisPro* (version 1.171.38.43)[4]. The crystal structures were solved by charge flipping algorithm using *SUPERFLIP*32[5] and refined based on the spherical-atom approximation using *SHELXL2012*[6] included in the *WinGX* suite[7]. Packing diagrams were made using Mercury 4.1.2.[8]

**Single Crystal Neutron Laue Diffraction Experiments:** A 1.0 x 1.0 x 0.6 mm block-shaped single crystal of **BALAOA** was mounted to the ϕ axis of the KOALA Laue neutron

diffractometer which stands at an end of guide position at the OPAL Research Reactor of the Australian Nuclear Science and Technology Organization.[9] The crystal was slowly cooled by means of an Oxford Cryosystems COBRA™ to 285K at which temperature a set of 15 diffraction images exposed for 1200 s, separated by 14 sequential ϕ rotations of 13$^{o}$ and suitable for data reduction[10] was secured. However, the data to parameter ratio was not high (bound by the wavelength) for the neutron diffraction data set. We performed joint structural refinement using both our in-house X-ray diffraction data and the neutron diffraction data collected at KOALA beamline at the particular temperature (285 °C). Cell parameters values observed from X-ray diffraction experiments at each temperature were used to index the neutron diffraction data at those temperatures. Indexing of neutron diffraction data was in good agreement with X-ray diffraction data set. We solved the crystal structure using X-ray diffraction data set. We used the positional parameters and thermal parameters for all the non-hydrogen atoms as the starting model for the structural refinement using neutron diffraction data set in *WinGX* suite[7]. The neutron diffraction data was used to locate all the hydrogen atoms accurately and to get the accurate anisotropic thermal parameters of each hydrogen atom. Scaling between the anisotropic parameters of hydrogen atoms and non-hydrogen atoms were done carefully. The neutron crystal structure confirms the partial proton transfer from oxalic acid to the amine group of amino acids forming hemi-oxalate salt, and the geometry of the hydrogen bonding network around the water molecule became crystal clear.

**Thermogravimetric Analysis (TGA):** TGA was performed by placing a sample size of 3-6 mg using a Mettler Toledo TGA/SDTA851e/SF/1100 in a standard 80 µL aluminium pan. Samples were heated with a scan rate of 10 °C /min in the temperature range 30–500 °C with an air

purged at 50 mL/min was used for the analysis. Mettler Toledo STARe software (Version 8) was used for data analysis of thermograms.

**Gas Adsorption Studies:** The nitrogen gas adsorption measurements were carried out by employing Belsorp Max equipment at liquid $N_2$ temperature.

**Proton Conductivity Measurements ($\sigma_p$):** Proton conductivity measurements of the materials were carried out by using a two-probe AC impedance analysis under humidified conditions. Materials were made in the form of solid pellets by applying a pressure of 1000 psi for 2 min. Obtained uniform pellets were of thickness between 1.0 to 1.4 mm and 1.32665 $cm^2$ area. Impedance analysis was done by keeping solid pellets between two-electrode assemblies with stainless steel discs as electrodes and the whole setup was kept inside a temperature-controlled humidity chamber (SH-241, ESPEC Co. Ltd., Japan), which was also connected to a BioLogic® electrochemical work station (VMP-3). The sample was left to equilibrate at each condition for a minimum of 1 h or until a steady state was reached. In the course of the experiment, the electrochemical impedance measurements were performed in the frequency range of 1 MHz-0.1 Hz using an input voltage amplitude of 10 mV. The steps per decade was set to 6 points per decade.

Comparison of the proton conductivity using $H_2O$ and $D_2O$ was conducted in a home-built smaller demonstration chamber using 30 mL of $H_2O$ and $D_2O$, under 98% RH for reliable results. Both proton and deuteron conductivities were measured after saturating the pellets in $H_2O$ and $D_2O$, respectively, for 12 h. All the AC impedance data were fitted using an EC-Lab Software V10.19 using an equivalent circuit for all the systems. For details see supplementary information.

**Electrical Conductivity Measurements ($\sigma_e$):** Electrical conductivity measurements of the materials were carried out using a two-electrode setup in a BioLogic® electrochemical workstation (VMP-3). LSV measurements were done by sweeping the potential from -0.5 to 0.5V with a scan rate of 50 mV $s^{-1}$. For details see supporting information.

**Fabrication of membrane electrode assembly (MEA) using pelletized GLYOA:** Standard PEMFC protocol was adopted for the preparation of MEA. Briefly, pelletized GLYOA of diameter 2.7 cm and thickness 1.58 mm were sandwiched between the electrodes with Kapton as gasket by 0.25-ton pressure for 1 minute at room temperature by using a hydraulic press (CARVER, USA). The electrodes were prepared by brush coating the *state-of-the-art* Pt/C (40 wt.%, Johnson Matthey) catalyst slurry on the surface of the carbon gas diffusion layer (GDL). In the case of both anode and cathode, the Pt loading was maintained at 2 mg $cm^{-2}$. The effective area was 4.50 $cm^2$ in a circular shape. The single cell evaluation of the as-prepared MEA was performed by using a standard fixture (Fuel Cell Technologies). The polarization analysis was carried out in a humidified $H_2$ and $O_2$ environment where the gas flow was 200 sccm and 300 sccm to the anode and cathode, respectively. All the analyses were performed at 60 °C cell temperature and 100 % relative humidity condition without applying any backpressure.

## Conductivity Measurements

**Proton Conductivity Measurements ($\sigma_p$):**

In the case of the **BALAOA** and **GLYOA** samples, the proton conductivity is measured at different temperatures (from 30 °C to 60 °C) under 95% RH, while for **LEUOA**, the proton

conductivity is measured at temperatures ranging from 30 °C to 80 °C under 95% RH. The proton conductivity is calculated using the Pouillet's equation, $\sigma_p = L / (R \times A)$, where **σ** is the conductivity (S $cm^{-1}$), **L** is the thickness of the measured sample (cm), and **A** is the electrode area ($cm^2$). The resistance is calculated using the high-frequency intercept of the Nyquist plot measured by the impedance spectroscopy.

Activation energy corresponding to proton conduction at different temperatures were determined by using the formula below,

$$\sigma = \sigma_o e^{\left(\frac{-E_a}{kT}\right)}$$

Where **σ** and $\sigma_o$ indicate conductivity and pre-exponential factor, respectively. **T** represents the absolute temperature in Kelvin, $E_a$ denotes the activation energy and **k** indicates the Boltzmann constant.

Comparison of the proton conductivity using $H_2O$ and $D_2O$ was conducted in a home-built smaller demonstration chamber using 30 mL of $H_2O$ and $D_2O$, under 98% RH for reliable results. Both proton and deuteron conductivities were measured after saturating the pellets in $H_2O$ and $D_2O$, respectively, for 12 h.

All the AC impedance data were fitted using an EC-Lab Software V10.19 using an equivalent circuit for all the systems. The Nyquist plots of **BALAOA** and **GLYOA** samples were fitted using the equivalent circuit below.

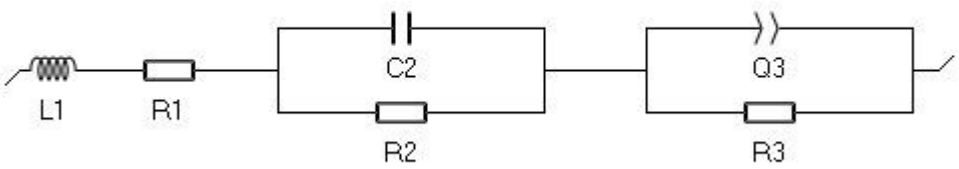

Where **L1**: Inductance; **R1**, **R2** &**R3**: Resistance; **C2**: Capacitance, and **Q3**: Constant phase element.

On the other hand, the Nyquist plot of **LEUOA** sample was fitted with the equivalent circuit below

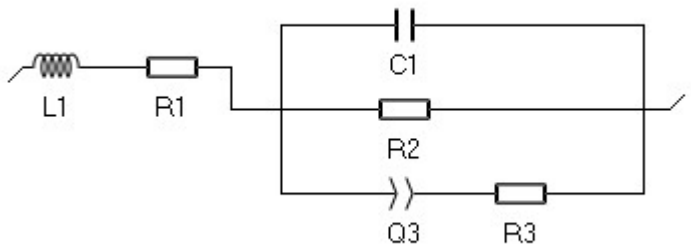


Where **L1**: Inductance; **R1**, **R2** &**R3**: Resistance; **C2**: Capacitance, and **Q3**: Constant phase element.

**Electrical Conductivity Measurements ($\sigma_e$):**

Electrical conductivity calculated by using this formula.

$$\sigma = \frac{i}{V} \times \frac{L}{A}$$

Where, ***σ*** is the conductivity (S $cm^{-1}$), ***L*** is the thickness of the measured sample (cm), ***A*** is the electrode area ($cm^2$) and ***i*** is the current (Ampere) corresponds to 0.4 V potential.

## Results:

### Crystal Structure and Hydrogen Bonding Network:

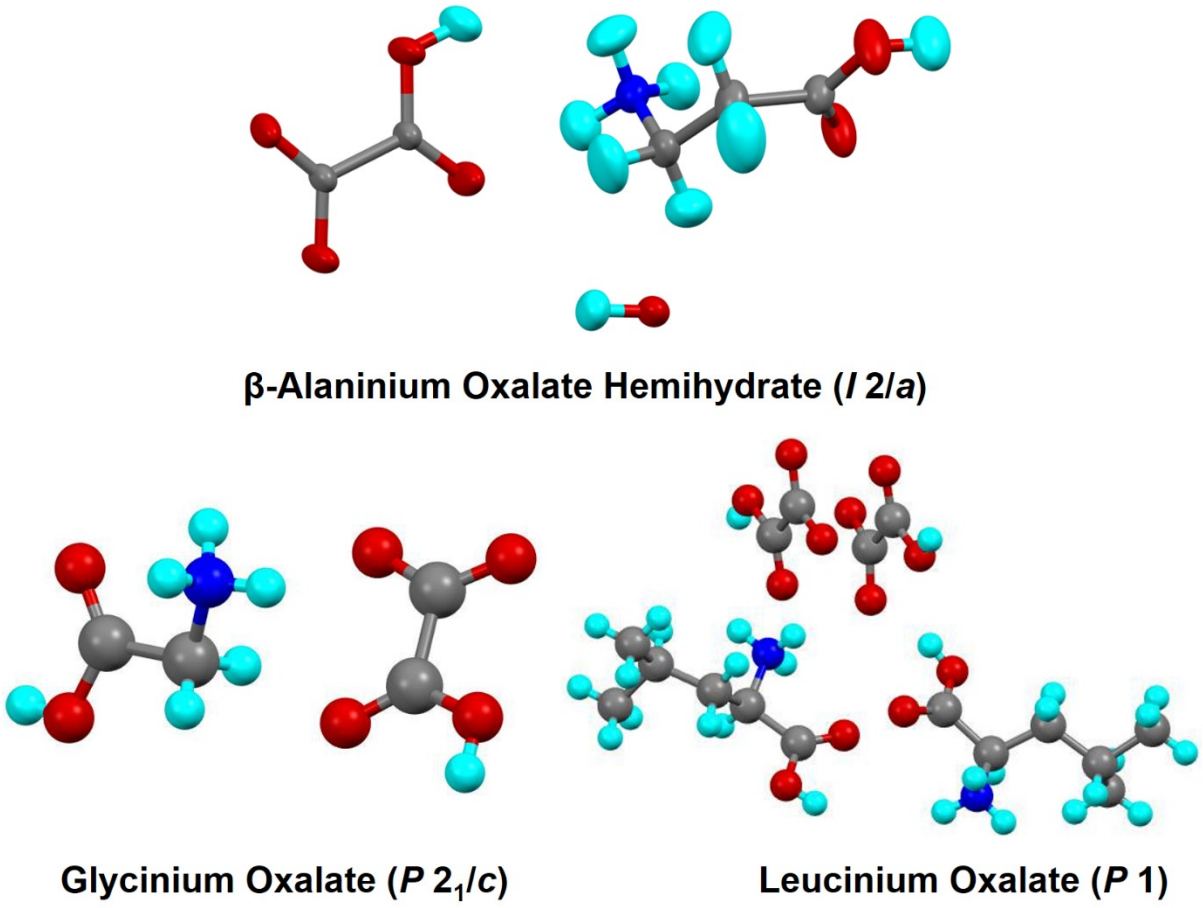


**Figure S1**: Asymmetric unit of β-Alaninium oxalate hemihydrate (**BALAOA**), Glycinium oxalate (**GLYOA**), and L-Leucinium oxalate (**LEUOA**). Colour code of atoms: Carbon (grey), Hydrogen (cyan), Nitrogen (blue), and Oxygen (red).

**Table S1**: Crystallographic table of X-ray structure and Neutron structure of **BALAOA**.

| | **BALAOA**<br>X-ray structure | **BALAOA**<br>Neutron structure |
|---|---|---|
| Formula | $C_3H_8NO_2$, $C_2HO_4$, $0.5H_2O$ | $C_3H_8NO_2$, $C_2HO_4$, $0.5H_2O$ |
| T(K) | 285 (2) | 285 (2) |
| Space Group | *I* 2/*a* | *I* 2/*a* |
| a (Å) | 20.666(8) | 20.666(8) |
| b (Å) | 5.6892(16) | 5.6892(16) |
| c (Å) | 14.016(4) | 14.016(4) |
| β (deg) | 102.279(6) | 102.279(6) |
| Volume ($Å^3$) | 1610.2(9) | 1610.2(9) |
| Z | 8 | 8 |
| Observed Reflections | 9403 | 2003 |
| Unique Reflections | 2453 | 1331 |
| No. of Parameters | 154 | 204 |
| Completeness (%) | 99.8 | 73.2 |
| $R_1$ [ I>2σ(I)](%) | 3.97 | 5.64 |
| $R_1$ (all data)(%) | 4.22 | 11.35 |
| GooF | 1.042 | 1.072 |
| $\Delta\rho_{min,max}$ | -0.263, 0.312(e $Å^{-3}$) | -0.433, 0.432(fm $Å^{-3}$) |
| CCDC No. | 2041757 | 2132573 |

[CCDC **2041757**, **2132573** contain the supplementary crystallographic data for this paper. These data can be obtained free of charge from the Cambridge Crystallographic Data Centre via www.ccdc.cam.ac.uk/data_request/cif.]

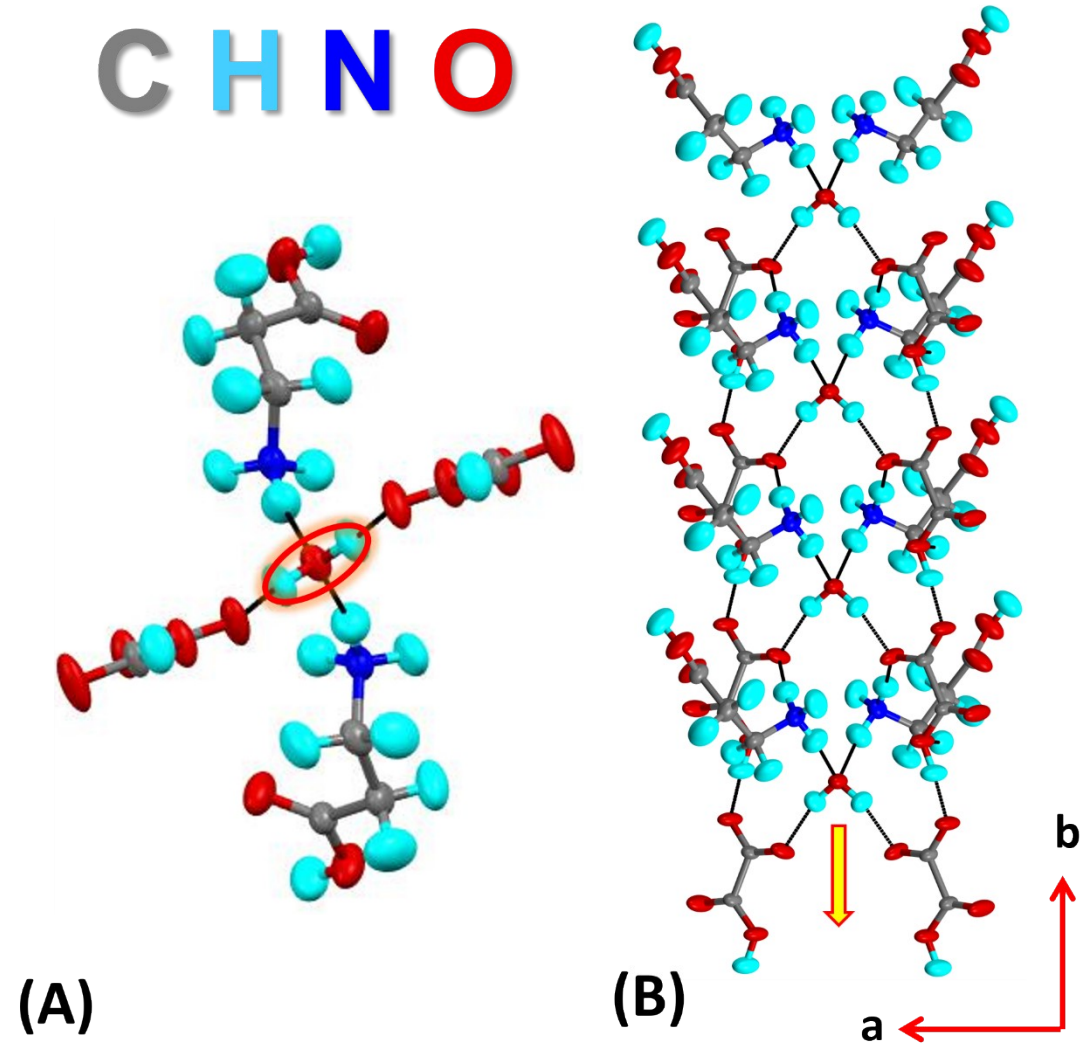


**Figure S2**: Supramolecular architecture of H-bonding network in **BALAOA** (**A** and **B**). **(A)** Dual role of water molecule (highlighted in red) in forming N-H•••O (as bond acceptor) and O-H•••O (as bond donor) hydrogen bonding. **(B)** Hydrogen bonded network around the water molecules, forming molecular column about the 2-fold axis (shown in yellow arrow).

**Table S2**: Hydrogen bond details in **BALAOA** crystal structure obtained from single-crystal Neutron Laue diffraction experiments.

| Donor(D)---H•••Acceptor(A) | D-H (Å) | H•••A (Å) | D-H•••A (Å) | < D-H•••A (°) |
|---|---|---|---|---|
| O3---H1O3•••O6 | 1.025 (3) | 1.557 (3) | 2.579 (2) | 175.1 (3) |
| O1W---H1W•••O5 | 0.964 (4) | 1.768 (4) | 2.704 (3) | 162.3 (3) |
| N1---H1N1•••O4 | 1.019 (4) | 2.475 (5) | 3.265 (3) | 134.0 (3) |
| N1---H1N1•••O6 | 1.019 (4) | 1.938 (5) | 2.849 (3) | 147.3 (3) |
| N1---H2N1•••O5 | 1.026 (4) | 1.856 (4) | 2.860 (2) | 165.2 (3) |
| N1---H3N1•••O1W | 1.037 (4) | 1.768 (4) | 2.790 (2) | 167.7 (4) |
| O1---H1O1•••O2 | 0.991 (5) | 1.665 (5) | 2.654 (3) | 175.9 (4) |
| C3---H1C3•••O4 | 1.085 (5) | 2.256 (5) | 3.286 (3) | 157.6 (4) |

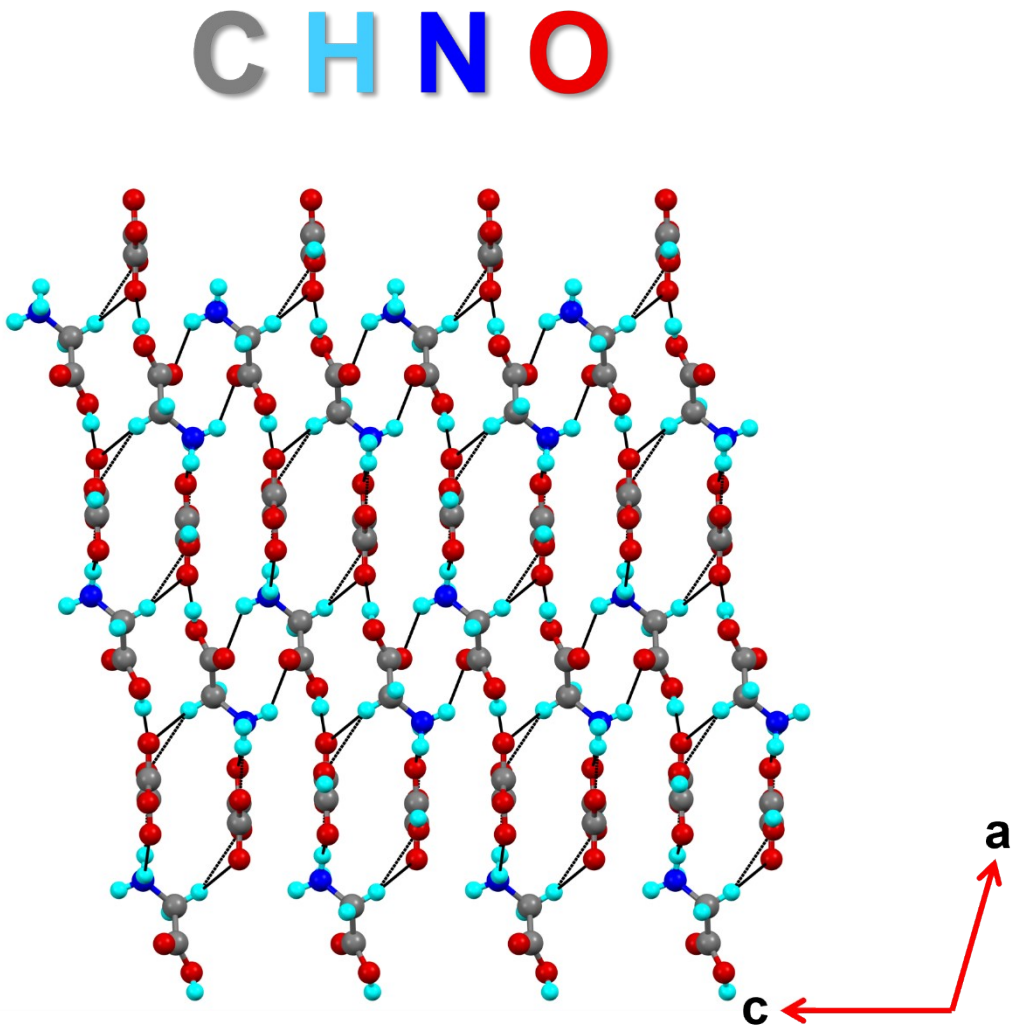


**Figure S3**: Supramolecular architecture of H-bonding network in **GLYOA**. Stacking of molecular layers through hydrogen bonding network along the '*c*' axis.

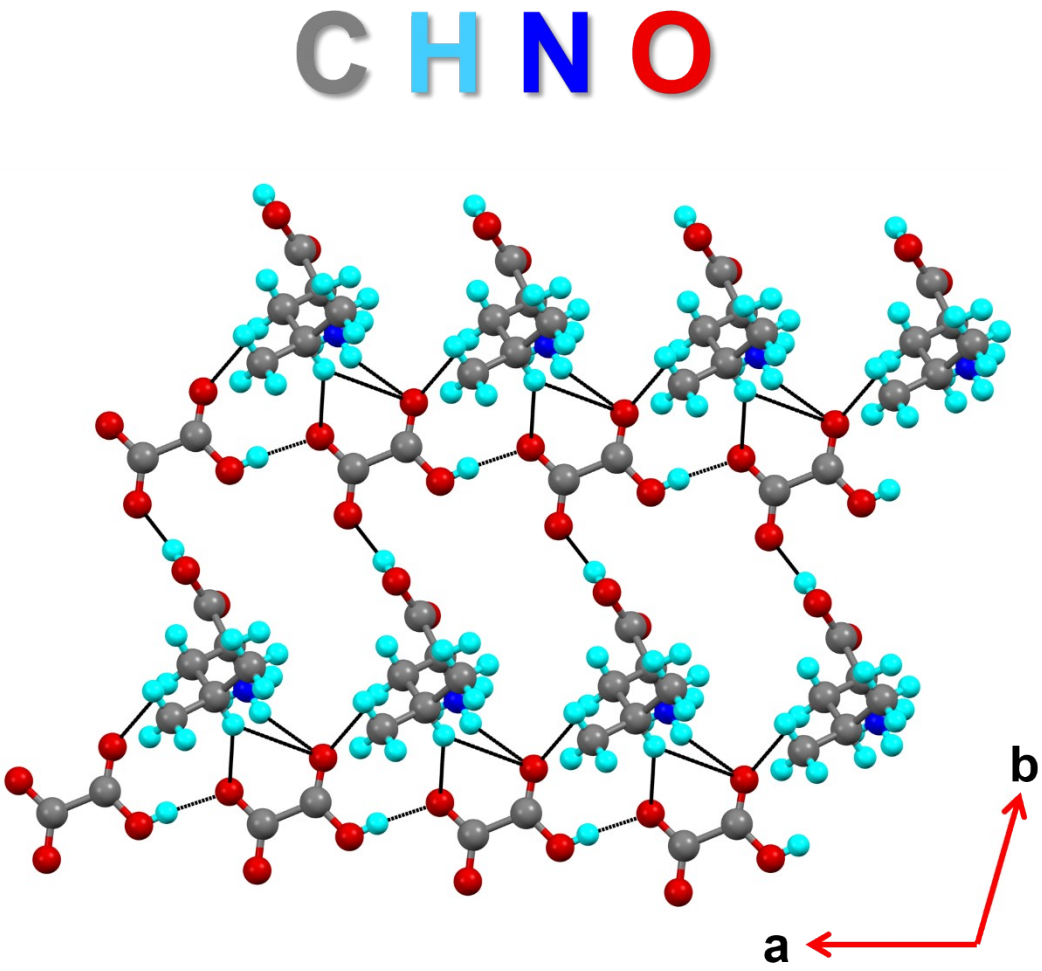


**Figure S4**: Supramolecular architecture of H-bonding network in **LEUOA.** A molecular layer of hydrophilic hydrogen bonding network as viewed down to the '*c*' axis.

**Thermogravimetric Analysis (TGA):** TGA analysis (**Figure S5A**) suggests that the compound is stable from room temperature to 100°C (a reasonable window for the PEM operations). Dehydration occurs around 100 °C and the anhydrous material is stable beyond 200 °C, indicating that stable hydrogen bond networks would exist even in the anhydrous form of the salt cocrystal. In fact, this observation inspired the synthesis of anhydrous **LEUOA** and **GLYOA** salt cocrystals, both compounds exhibiting high proton conductivity and higher thermal stability (stable up to 200 °C and 175 °C, respectively) (**Figure S5B** and **S5C**).

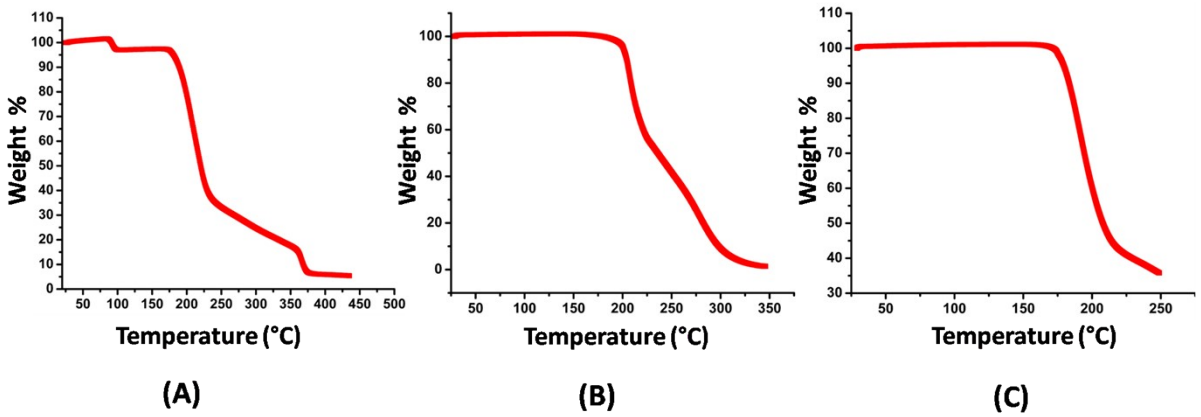


**Figure S5**: **(A)** TGA pattern of **BALAOA** shows the dehydration temperature is around 100 °C. **(B)** TGA pattern of anhydrous salt cocrystals of **LEUOA**. **(C)** TGA pattern of anhydrous salt cocrystals of **GLYOA**.

**Powder X-ray Diffraction (PXRD):** Bulk powder materials of **BALAOA**, **GLYOA**, and **LEUOA** were prepared by liquid assisted grinding of the constituents in the stoichiometric ratio (1:1) to carry out the Electrochemical Impedance Spectroscopy (EIS) analysis for proton conductivity measurements. The phase purity of each of these powder samples was characterized by profile fitting of the room temperature PXRD data (**Figure S6**).

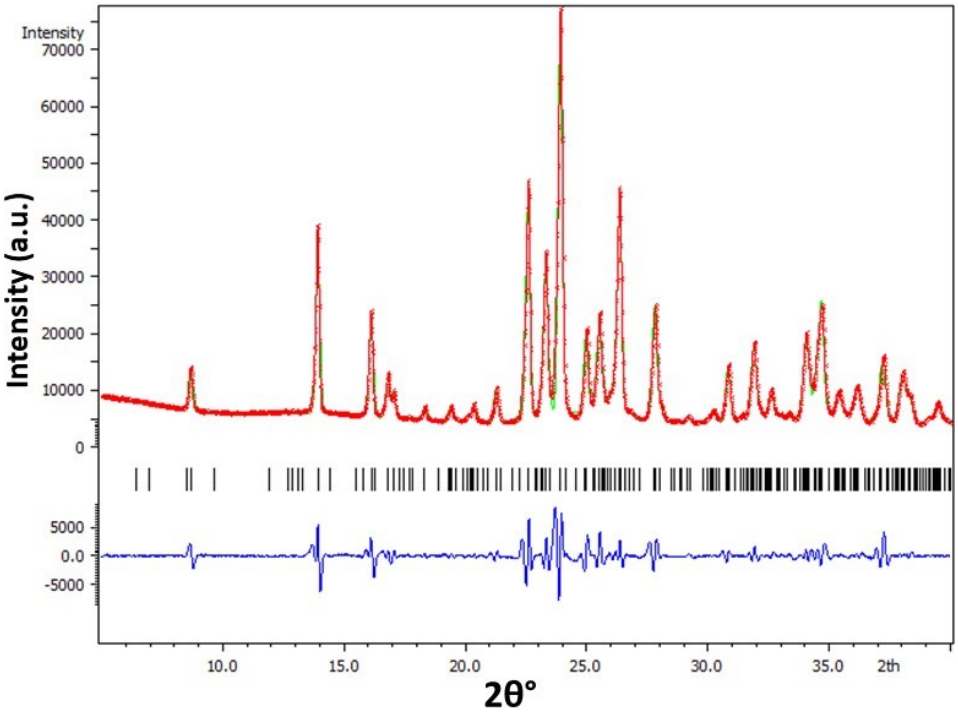


**(A)**

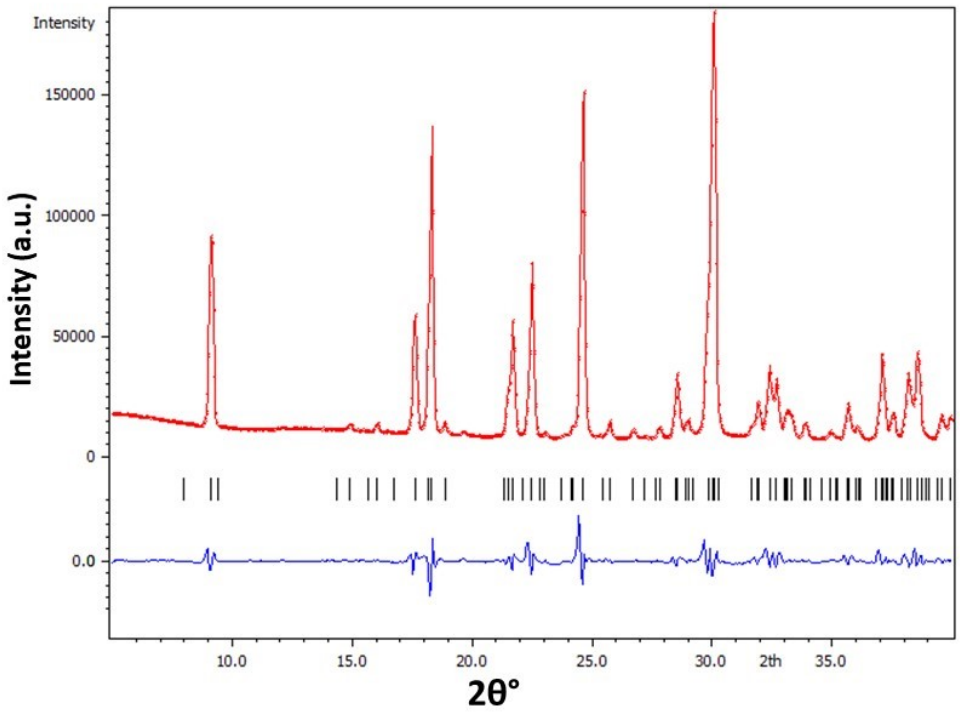


**(B)**

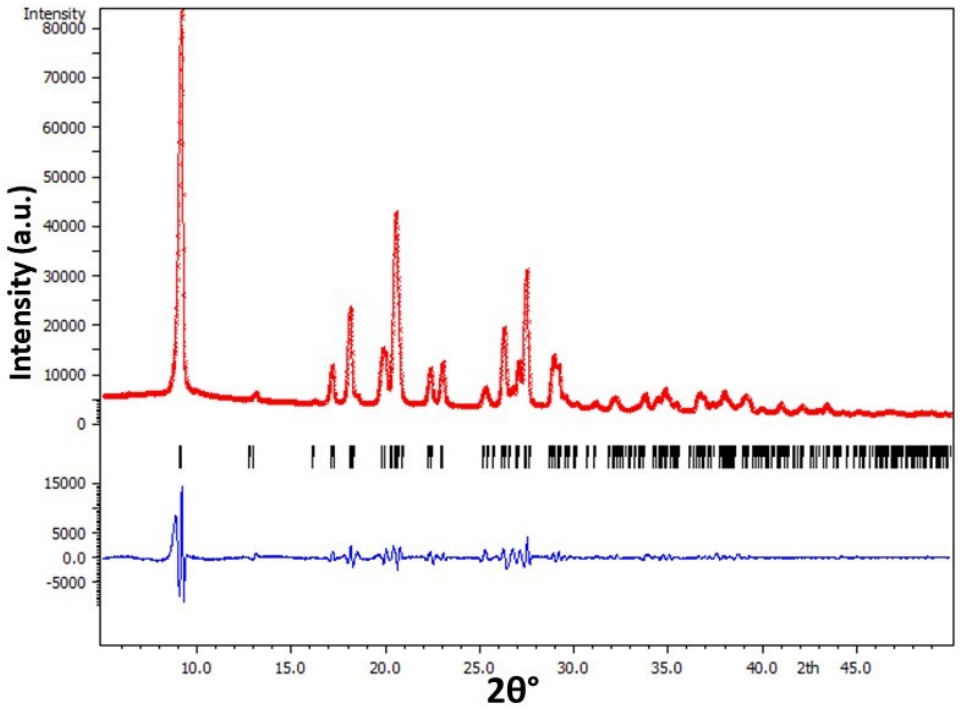


**(C)**

**Figure S6**: Profile fitting of the PXRD patterns of (**A**) **BALAOA** (Rp=5.2%), (**B**) **GLYOA** (Rp=3.7%), and (**C**) **LEUOA** (Rp=6.3%). No impurity was observed in any of the samples. Red: calculated, Green: Observed, Blue: difference.

**Proton Conductivity Measurements:**

Electrochemical Impedance Spectroscopy (EIS) technique was employed on pelletized samples (1.0 mm to 1.4 mm) of each material with controlled humidity and temperature to analyse the proton-conducting behaviour. The Nyquist plots show that the bulk resistance of these samples is very low and the high-frequency intercept of the Nyquist plot was considered as the bulk resistance in all the cases. It is to be noted that the usually dominant appearance of semi-circle formation in the Nyquist plot is not observed in any of the systems. The disappearance of the semi-circle is accounted for the decrease in the time constant (τ) value, which depends on the bulk resistivity of the samples as previously explained by Kitagawa et al.[11]

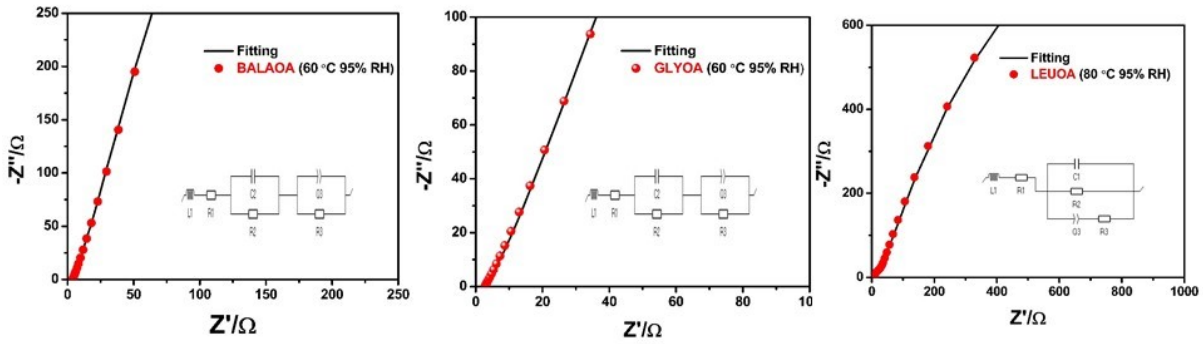


**Figure S7**: Nyquist plot fitting of **BALAOA** (left), **GLYOA** (middle), and **LEUOA** (right).

**Table S3**: Summary of two-probe AC impedance measurements of **BALAOA** under different temperatures and 95% relative humidified (RH) conditions (1.08 mm thick pellet).

| Sl. No | Condition | Resistance (Ohm) | Conductivity (S $cm^{-1}$) |
|---|---|---|---|
| 1 | 30 °C, 95% RH | 13.4 | $6.08 \times 10^{-3}$ |
| 2 | 40 °C, 95% RH | 8.8 | $9.25 \times 10^{-3}$ |
| 3 | 50 °C, 95% RH | 5.3 | $1.54 \times 10^{-2}$ |
| 4 | 60 °C, 95% RH | 3.3 | $2.43 \times 10^{-2}$ |

**Table S4**: Summary of two-probe AC impedance measurements of **BALAOA** under different humidified (RH) conditions and at 60 °C (1.35 mm thick pellet)

| Sl. No | Condition | Resistance (Ohm) | Conductivity (S $cm^{-1}$) |
|---|---|---|---|
| 1 | 60 °C, 40% RH | 22 | $4.63 \times 10^{-3}$ |
| 2 | 60 °C, 50% RH | 20 | $5.09 \times 10^{-3}$ |
| 3 | 60 °C, 60% RH | 18 | $5.65 \times 10^{-3}$ |
| 4 | 60 °C, 70% RH | 16.5 | $6.17 \times 10^{-3}$ |
| 5 | 60 °C, 80% RH | 13.6 | $7.48 \times 10^{-3}$ |
| 6 | 60 °C, 95% RH | 4.2 | $2.42 \times 10^{-2}$ |

**Table S5**: Summary of two-probe AC impedance measurements of **GLYOA** under different temperatures and 95% relative humidified (RH) conditions (1.03 mm thick pellet).

| Sl. No | Condition | Resistance (Ohm) | Conductivity (S $cm^{-1}$) |
|---|---|---|---|
| 1 | 30 °C, 95% RH | 6.06 | $1.28 \times 10^{-2}$ |
| 2 | 40 °C, 95% RH | 3.66 | $2.12 \times 10^{-2}$ |
| 3 | 50 °C, 95% RH | 3.19 | $2.43 \times 10^{-2}$ |
| 4 | 60 °C, 95% RH | 2.56 | $3.03 \times 10^{-2}$ |

**Table S6**: Summary of two-probe AC impedance measurements of **GLYOA** under different humidified (RH) conditions and at 60 °C (1.05 mm thick pellet).

| Sl. No | Condition | Resistance (Ohm) | Conductivity (S $cm^{-1}$) |
|---|---|---|---|
| 1 | 60 °C, 40% RH | 508 | $1.56 \times 10^{-4}$ |
| 2 | 60 °C, 50% RH | 385 | $2.06 \times 10^{-4}$ |
| 3 | 60 °C, 60% RH | 335 | $2.36 \times 10^{-4}$ |
| 4 | 60 °C, 70% RH | 288 | $2.75 \times 10^{-4}$ |
| 5 | 60 °C, 80% RH | 79 | $1.00 \times 10^{-3}$ |
| 6 | 60 °C, 95% RH | 2.6 | $3.04 \times 10^{-2}$ |

**Table S7**: Summary of two-probe AC impedance measurements of **LEUOA** under different temperatures and 95% relative humidified (RH) conditions (1.31 mm thick pellet).

| Sl. No | Condition | Resistance (Ohm) | Conductivity (S $cm^{-1}$) |
|---|---|---|---|
| 1 | 30 °C, 95% RH | 728 | $1.36 \times 10^{-4}$ |
| 2 | 40 °C, 95% RH | 483 | $2.04 \times 10^{-4}$ |
| 3 | 50 °C, 95% RH | 239 | $4.13 \times 10^{-4}$ |
| 4 | 60 °C, 95% RH | 57.3 | $1.72 \times 10^{-3}$ |
| 5 | 70 °C, 95% RH | 20.8 | $4.75 \times 10^{-3}$ |
| 6 | 80 °C, 95% RH | 8.3 | $1.19 \times 10^{-2}$ |

**Table S8**: Summary of two-probe AC impedance measurements of **LEUOA** under different humidified (RH) conditions and at 80 °C (1.18 mm thick pellet).

| Sl. No | Condition | Resistance (Ohm) | Conductivity (S $cm^{-1}$) |
|---|---|---|---|
| 1 | 80 °C, 40% RH | 1031 | $8.63 \times 10^{-5}$ |
| 2 | 80 °C, 50% RH | 763 | $1.17 \times 10^{-4}$ |
| 3 | 80 °C, 60% RH | 603 | $1.48 \times 10^{-4}$ |
| 4 | 80 °C, 70% RH | 257 | $3.46 \times 10^{-4}$ |
| 5 | 80 °C, 80% RH | 84 | $1.06 \times 10^{-3}$ |
| 6 | 80 °C, 95% RH | 7.7 | $1.16 \times 10^{-2}$ |

**Electronic Conductivity, Stability,** and **Gas Permeability:** One of the important features of a potential PEM is its poor electronic conductivity ($\sigma_e$). The conduction of electrons through the PEM reduces the efficiency of the fuel cells. The $\sigma_e$ values observed for **BALAOA**, **GLYOA**, and **LEUOA** systems are negligible and are of the order $10^{-8}$ S $cm^{-1}$, making them promising PEMs for fuel cell application (**Figure S8A**). Additionally, to test the stability of the samples, AC impedance measurements were carried out at the extreme condition. No drop in proton conductivity was observed for all three systems (**Figure S8B**) even after 10 hours. Furthermore, the high proton conductivity values of these simple materials prompted us to measure their gas permeability. The BET adsorption isotherms show negligible uptake of $N_2$ gas in all of the three materials (**Figure S9**), which confirms the non-porous nature of these materials.

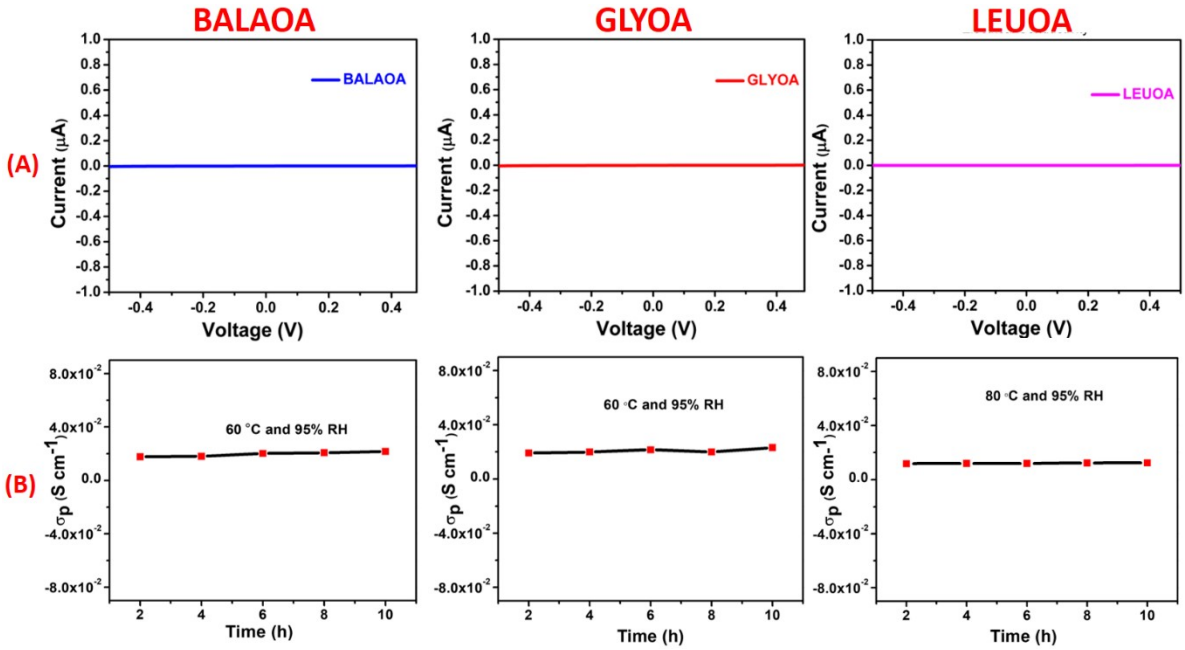


**Figure S8**: (**A**) Current vs. voltage profiles. (**B**) Time-dependent stability tests.

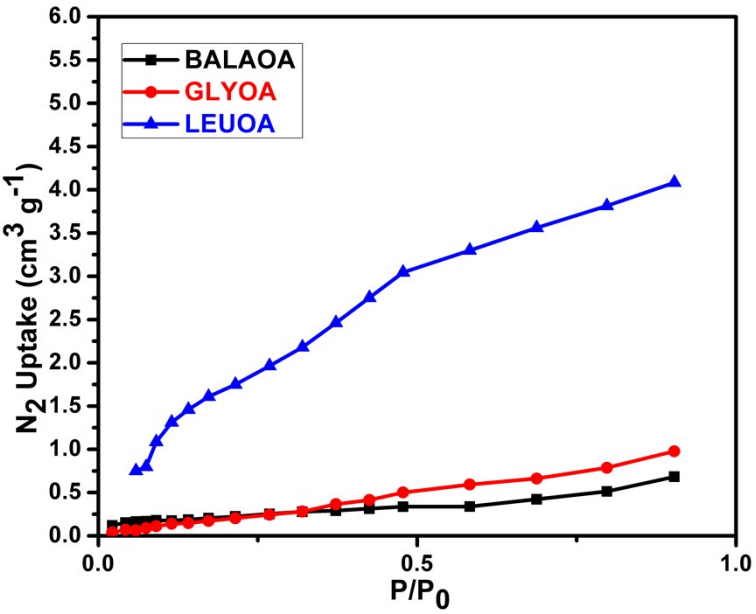


**Figure S9:** BET $N_2$ adsorption isotherms for all three compounds at liquid $N_2$ temperature.

**Fuel Cell Measurements:**

The membrane electrode assembly (MEA) was made up of pelletized **GLYOA** as the proton exchange material. The MEA with an active area of 4.50 $cm^2$ was prepared by using *state-of-the-art* Pt/C (40 wt. %) coated gas diffusion as both the cathode and

anode (**Figure S10**). The Pt loading was maintained as 2 mg $cm^{-2}$ on both electrodes. It is important to note that membrane thickness plays a crucial role in determining the MEA performance.[12] Although, the single-cell device performance of **GLYOA** is not competent with polymer based thin membranes (usually 50 μm compared to the present 1580 mm),[13–16] the power density observed is promising compared to other reported pellet based proton conducting fuel cells.[17,18] Therefore, the fuel cell polarization study validates the functioning of **GLYOA** as an efficient proton conducting material.

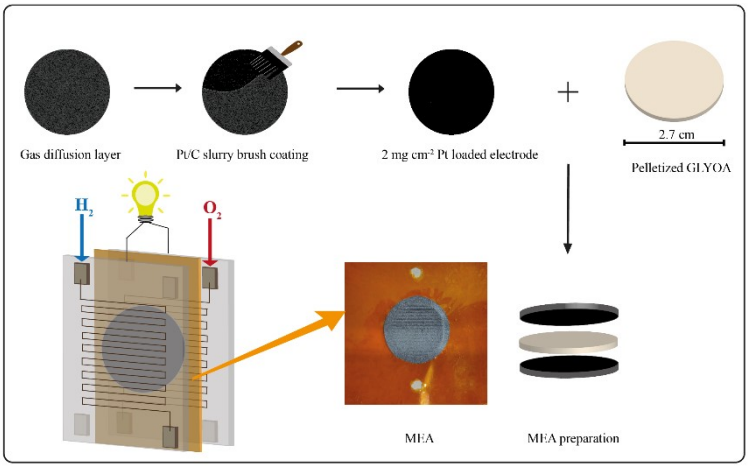


**Figure S10:** Schematic representation of fabrication of membrane electrode assembly (MEA) using pelletized **GLYOA** as a solid electrolyte.

**Table S9:** Comparison of proton conductivity values of **GLYOA**, **BALAOA**, and **LEUOA** with other reported proton conducting materials.

| No. | Compound | Conditions | Proton conductivity ( S cm-1) | Reference |
|---|---|---|---|---|
| 1 | H2SO4@MIL-101-SO3H (3M) | 70 °C, 90% RH | 1.82 | *ACS Energy Letters* **2017**, *2*, 2313-2318 |
| 2 | H2SO4@MIL-101 (3M) | 70 °C, 90% RH | $6.09 \times 10^{-1}$ | *ACS Energy Letters* **2017**, *2*, 2313-2318 |
| 3 | Nafion | 80 °C, 98% RH | ~$1 \times 10^{-1}$ | *J. Polym. Sci., Part B: Polym. Phys.* **2011**, *49*, 1437-1445 |
| 4 | PSM1 (UiO-66-NH-$SO_3H$) | 80 °C, 98% RH | $1.64 \times 10^{-1}$ | *ACS Appl. Mater. Interfaces* 2019, 11, 13423–13432 |
| 5 | UiO-66(SO3H)2 | 80 °C, 90% RH | $8.4 \times 10^{-2}$ | *Angew. Chem. Int. Ed.* **2015**, *54*, 5142-5146. |
| 6 | TJU-102 | 90 °C, 98% RH | $5.26 \times 10^{-2}$ | *Chem. Mater.* **2019**, *31*, 8494–8503. |
| 7 | Fe-CAT-5 | 25 °C, 98% RH | $5.0 \times 10^{-2}$ | *J. Am. Chem. Soc.* **2015**, *137*, 15394–15397. |
| 8 | PCMOF-10 | 70 °C, 95% RH | $3.55 \times 10^{-2}$ | *J. Am. Chem. Soc.* **2015**, *137*, 7640-7643 |
| 9 | Im@MOF-808 | 65 °C, 99% RH | $3.45 \times 10^{-2}$ | *ACS Appl. Mater. Interfaces* **2019**, *11* , 9164–9171. |
| 10 | BIP | 95 °C, 95% RH | $3.2 \times 10^{-2}$ | *J. Am. Chem. Soc* **2019**, *141*, 14950. |
| 11 | **GLYOA** | **60 °C, 95% RH** | **$3.03 \times 10^{-2}$** | **This Work** |
| 12 | **BALAOA** | **60 °C, 95% RH** | **$2.42 \times 10^{-2}$** | **This Work** |
| 13 | CPOS-2 | 60 °C, 98% RH | $2.2 \times 10^{-2}$ | *Angew. Chemie Int. Ed.* **2018**, *57*, 5345–5349 |
| 14 | H+@Ni2(dobdc)(H2O)2 (pH = 1.8) | 80 °C, 95% RH | $2.2 \times 10^{-2}$ | *Angew. Chem. Int. Ed.* **2014**, *53*, 8383–8387 |
| 15 | PCMOF21/2 | 85 °C, 90% RH | $2.1 \times 10^{-2}$ | *J. Am. Chem. Soc.* **2013**, *135*, 963-966. |
| 16 | HOF-GS-11 | 30 °C, 95% RH | $1.8 \times 10^{-2}$ | *Angew. Chem. Int. Ed.* **2016**, *55*, 10667-10671. |
| 17 | **LEUOA** | **80 °C, 95% RH** | **$1.19 \times 10^{-2}$** | **This Work** |
| 18 | CPOS-1 | 60 °C, 98% RH | $1.0 \times 10^{-2}$ | *Angew. Chemie Int. Ed.* **2018**, *57*, 5345–5349 |
| 19 | H2SO4@MIL-101 | 150 °C, 0.13% RH | $1.0 \times 10^{-2}$ | *J. Am. Chem. Soc.* **2012**, *134*,15640-15643. |
| 20 | (NH4)2(H2adp)[Zn2(ox)3]·3H2O | 25 °C, 98% RH | $0.8 \times 10^{-2}$ | *J. Am. Chem. Soc.* **2009**, *131*, 9906-9907 |
| 21 | HOF-GS-10 | 30 °C, 95% RH | $0.75 \times 10^{-2}$ | *Angew. Chem. Int. Ed.* **2016**, *55*, 10667-10671. |

## References


1 R. V Krishnakumar, M. Subha Nandhini and S. Natarajan, *Acta Crystallogr. Sect. E Struct. Reports Online*, 2002, **58**, o117–o119.

2 M. Subha Nandhini, R. V Krishnakumar and S. Natarajan, *Acta Crystallogr. Sect. C*, 2001, **57**, 115–116.

3 K. Rajagopal, R. V Krishnakumar, M. Subha Nandhini, R. Malathi, S. S. Rajan and S. Natarajan,

*Acta Crystallogr. Sect. E Struct. Reports Online*, 2003, **59**, o878–o880.

4 O. D. Rigaku, *Rigaku Oxford Diffr. Ltd, Yarnton, Oxfordshire, Engl.*

5 L. Palatinus and G. Chapuis, *J. Appl. Crystallogr.*, 2007, **40**, 786–790.

6 G. M. Sheldrick, *Acta Crystallogr. Sect. C Struct. Chem.*, 2015, **71**, 3–8.

7 L. J. Farrugia, *J. Appl. Crystallogr.*, 2012, **45**, 849–854.

8 C. F. Macrae, P. R. Edgington, P. McCabe, E. Pidcock, G. P. Shields, R. Taylor, M. Towler and J. V. D. Streek, *J. Appl. Crystallogr.*, 2006, **39**, 453–457.

9 A. J. Edwards, .

10 R. Piltz, in *ACTA CRYSTALLOGRAPHICA A-FOUNDATION AND ADVANCES*, INT UNION CRYSTALLOGRAPHY 2 ABBEY SQ, CHESTER, CH1 2HU, ENGLAND, 2011, vol. 67, pp. C155–C155.

11 D. Umeyama, S. Horike, M. Inukai, Y. Hijikata and S. Kitagawa, *Angew. Chemie*, 2011, **123**, 11910–11913.

12 N. K. Nadermann, E. M. Davis, K. A. Page, C. M. Stafford and E. P. Chan, *Adv. Mater.*, 2015, **27**, 4924–4930.

13 L. Cao, H. Wu, Y. Cao, C. Fan, R. Zhao, X. He, P. Yang, B. Shi, X. You and Z. Jiang, *Adv. Mater.*, 2020, **32**, 2005565.

14 W. Wu, Y. Li, J. Liu, J. Wang, Y. He, K. Davey and S. Qiao, *Adv. Mater.*, 2018, **30**, 1707516.

15 G. He, M. Xu, J. Zhao, S. Jiang, S. Wang, Z. Li, X. He, T. Huang, M. Cao and H. Wu, *Adv. Mater.*, 2017, **29**, 1605898.

16 R. Thimmappa, M. Gautam, M. C. Devendrachari, A. R. Kottaichamy, Z. M. Bhat, A. Umar and M. O. Thotiyl, *ACS Sustain. Chem. Eng.*, 2019, **7**, 14189–14194.

17 H. B. Aiyappa, S. Saha, P. Wadge, R. Banerjee and S. Kurungot, *Chem. Sci.*, 2015, **6**, 603–607.

18 D. B. Shinde, H. B. Aiyappa, M. Bhadra, B. P. Biswal, P. Wadge, S. Kandambeth, B. Garai, T. Kundu, S. Kurungot and R. Banerjee, *J. Mater. Chem. A*, 2016, **4**, 2682–2690.